VISIBLE-LIGHT SENSITIVE PHOTOCATALYSTS BY NITROGEN MODIFICATION FOR VOC DESTRUCTION

Walter Den[1], Hsunling Bai[2]

1. Department of Environmental Science, Tunghai University, wden@mail.thu.edu.tw
2. Institute of Environmental Engineering, National Chiao Tung University, hlbai@mail.nctu.edu.tw

ABSTRACT

Gas-phase photocatalysis using titanium dioxide (TiO_2) has been regarded as an attractive technology for the control of VOC emissions. However, TiO_2 requires ultraviolet irradiation exceeding the bandgap energy of 3.0 eV (wavelength < 400 nm), hence effectively eliminating the utilization of solar and interior lighting as a source of photo-activation energy. Recently, a number of studies have demonstrated that incorporation of anionic species into the Ti^{3+} sites induces an oxygen vacancy band just below the conduction band edge, thereby narrowing the bandgap energy for photo-excitation of TiO_2. In this study, we have characterized the nitrogen-modified anatase TiO_2 powders by two different approaches – the first being calcination of the powders in an NH_3-enriched atmosphere, and the second being surface treatment by radio-frequency (RF) plasma in N_2 environment. The optimum treatment conditions for both approaches were evaluated based on the light absorptivity in the visible spectrum (wavelength<550nm). Analyses by X-ray photoelectron spectroscopy showed distinct peaks (396 eV and 400 eV) that typified the presence of N-bonding, with the plasma-treated powders exhibiting more intense peak at 396 eV. The difference in the surface N-bonding may have resulted in different absorptivities of the doped TiO_2 samples, which indicated a substantially higher visible-light absorptivity by the plasma-treated TiO_2. Furthermore, the photocatalytic function of the doped TiO_2 powders was examined in a continuous-flow or batch chambers subjected to monochromic UV (365 nm) or visible (450-550 nm) light irradiations at adjustable intensities. Both nitrogen-modified samples showed significant decomposition (ca. 40% and ca. 65% destruction efficiencies) of isopropanol vapor (< 1500 ppmv) under visible light.

INTRODUCTION

Gas-phase photocatalytic oxidation using semiconductor materials has been regarded as an attractive technology for the control of volatile organic compound (VOC) emissions. In photocatalytic oxidation process, the incident photons possessing energies greater than the solid bandgap are absorbed by the catalysts, causing excitation of valence electrons into the conduction band. This photo-excitation generates electron-hole pairs that migrate to surface sites where redox reaction occurs with the adsorbed organic molecules. Among many candidates, titanium dioxide (TiO_2, an n-type semiconductor) unquestionably draws the most attention because of its chemical stability and commercial availability with low costs. However, TiO_2 requires ultraviolet (UV) radiation whose energy must exceed the bandgap of 3.0 eV ($\lambda < 400$ nm), hence effectively eliminating the utilization of solar and interior lighting as a source of photo-activation energy.

Extensive research efforts have been devoted in the past decade to develop titanium oxide-based semiconductor photocatalysts that are sensitive to visible light. For this purpose, attempts have been made to modify the TiO_2 bandgap state by inserting cationic metal ions such as Pt, Al, Sb, Fe, Ag, Cr into the Ti^{4+} lattice sites of in the TiO_2 structure. This creates intra-bandgap states close to the conduction or valence band edges, and effectively "narrows" the bandgap and the energy needed for photo-excitation. This type of modified TiO_2 photocatalysts have indeed been demonstrated with enhanced absorbance band well within visible-light region (λ>450 nm). The major drawback of this approach, however, is that the metal-doped induced states in the TiO_2 bandgap can also be efficient charge recombination centers. Coupled with the thermal instability associated with the doped metals (Choi, 1994), some reservation has been raised about their long-term photocatalytic activity. Another approach is to introduce anionic species such as N (Sato, 1986; Asahi et al., 2001), S (Umebayashi et al., 2003; Ohno et al., 2003), and F (Hittori et al., 1998; Yu et al., 2002) into the Ti^{3+} sites, creating a slightly reduced form of TiO_2 by inducing an oxygen vacancy. This vacancy-induced band just below the conduction band edge not only reduces the photo-excitation energy due to the narrowing bandgap, but also facilitates the transport of photocarriers to the surface for photodegradation. For example, Asahi et al. (2001) obtained a nitrogen-doped titania upon heating anatase powder in an atmosphere of a mixture of ammonia (NH_4) and argon (Ar). The resultant product, assigned as $TiO_{2-x}N_x$, was capable of decoloring methylene blue by irradiating at wavelengths between 350-500 nm.

The results from the numerous studies mentioned above all point to the direction that the narrow band states of the modified titania powders or thin films create a red-shift in the photo-absorption spectrum that crosses the visible-light barrier. Whether this red-shift phenomenon can effectively translate to the application of emission control as efficient as the

undoped TiO_2 is still questionable. In this study, we intent not only to examine the physicochemical and optical properties of the nitrogen-doped titania, but also to evaluate the photocatalytic activity of the N-doped titania in a flow-through reactor for decomposition of isopropanol (IPA) irradiating at both UV (λ=365 nm) and visible light regions.

MATERIALS AND METHODS

N-doped TiO_2 preparation

Commercially available TiO_2 powder (ST-01, Ishihara Sangyo Kaisha Ltd., Japan) was used as the starting material to be modified by two different methods, namely thermal calcinations and RF plasma treatment. For the former method, powders were weighted (3.0 g) and placed on the bottom of a 25-cm quartz draft tube, whose lower half was extended into an electric furnace (Barnstead International Inc., USA). 300 mL min^{-1} of dry air mixtures containing NH_4 (50% or 67% v/v) were introduced into the draft tube, which was heated at 400, 500, and 600°C for at least 3 hours. This experimental apparatus ensures precise control of gas mixtures and uniform heating during TiO_2 annealing. The NH_3 modified powders are denoted as ST01-T400NH_3, ST01-T500NH_3, and ST01-T600NH_3, respectively. The powder samples were also annealed under air and N_2 flow to serve as controlled experiments. For the latter method, precisely 0.8 g of powders were fixed on a quartz disk through dissolution and desiccation, and placed in a RF plasma chamber (RF 13.56MHz, 300W maximum power output) equipped with heating sample holder (up to 400°C) and high-vacuum pump (1 mTorr). Purified nitrogen gas was metered (700 mL min^{-1}) and introduced into the chamber as the plasma and dopant gas. Plasma treatment duration was typically limited to ten minutes. The plasma-modified products under various plasma intensities are hereinafter denoted as ST01-P100N_2, ST01-P200N_2, and ST01-P300N_2). Both experimental methods are depicted schematically in Figure 1.

Characterization

The original and treated powder samples were characterized by a powder X-ray diffractometer (MXP18, MAC Science) with Cu Kα radiation at a scan rate of 0.05° s^{-1} between $0 < 2\theta < 100°$. The crystalline size was primarily measured by transmission electron microscopy, and also confirmed by following the Scherrer's formula associated with the peak characteristics of the XRD pattern. For TEM imaging, the powder samples were dispersed and deposited onto a carbon coated copper grid (200 mesh). The samples were examined with a Philips CM-200 TWIN electron microscope with an accelerating voltage of 200kV. The ultraviolet and visible absorption spectra of the powders were analyzed by an UV-visible spectrophotometer (UV-2501 PC, Shimadzu) augmented with an integrating sphere. The

Brunaur-Emmett-Teller (BET) surface area was determined using a Micromeritics ASAP 2100 analyzer with N_2 adsorption and desorption at 77K. Finally, the chemical composition of the nitrogen-containing TiO_2 was measured by X-ray photoelectron spectroscopy (XPS) using an ESCA (Physical Electronics, model PHi 1600) analyzer.

Photocatalysis experiments

The photocatalytic activity was evaluated by decomposition of IPA in a flow-through system featuring a light-sensitized packed column reactor (packing length, 6 cm; internal diameter, 4 cm). Approximately 50 g of clean glass beads (2 mm) was immerged in 5 wt% suspension of the doped TiO_2 powders for 12 hours, followed by 3 hours of drying (150°C) to complete the surface coating procedure. This coating procedure consistently maintained about 0.8 g of photocatalysts on the glass beads. A low-pressure mercury UV lamp (model TL/8W/05, Phillips Lighting), or a filtered fluorescent lamp (model TL/8W/840, Phillips Lighting) was secured in the middles of the tubular photocatalytic reactor to serve as the UV or visible light sources. The UV lamp, with an output power of 8W and primary output wavelength at 365 nm, produces an illumination intensity of 1.8 mW/cm^2 on the exterior wall without packing, and 0.1 mW/m^2 with TiO_2-coated packing. The fluorescent lamp produced an overall intention over 2000 Lux (2.4×10^{18} quanta$\cdot m^2 \cdot s^{-1}$) in the visible-light spectrum. For the photocatalytic experiments, IPA-contaminated air of various concentrations and flowrates was introduced into the reactor by controlling the vaporization temperature and air dilution ratio. Gaseous samples were withdrawn from the inlet and outlet ends of the reactor using a 1-mL air-tight glass syringe and immediately analyzed by a gas chromatograph (Varian 3900) equipped with a flame ionization detector and a 60m × 0.32mm fused silica capillary column.

RESULTS AND DISCUSSION

Material characterization of N-doped TiO_2 powders

The physical and chemical characteristics of the original (ST-01), thermal-doped TiO_2, and plasma-doped TiO_2 powders are summarized in Table 1. The XRD patterns shown in Figure 2 for both ST01-T600NH_3 and ST01-P300N_2 samples showed the distinct peaks of anatase TiO_2, with small peaks at $2\theta = 30.8°$ and 32.8° representing brookite phase also observed for ST01-T600NH_3. This result indicates that the powders remained a homogeneous anatase crystalline phase after calcination. Additionally, no peaks signaling TiN were observed from XRD patterns, implying that incorporation of nitrogen does not cause phase transformation or structural change in TiO_2. The width of the peaks, however, significantly sharpened as the temperature increased, suggesting the growth of crystalline size after

annealing. Based on the Scherrer's formula for the <101> anatase from the XRD patterns, the mean crystalline size was 10, 13, and 35 nm for ST-01, ST01-T400NH_3, and ST01-T600NH_3, respectively. Particles of ST01-P300N_2 were also in the proximity of 10 nm, indicating little change in crystalline size from the untreated powders.

The specific surface area of the calcinated powders was significantly reduced at higher annealing temperatures. Triplicate BET measurements indicated that the ratios of specific surface area between treated and untreated ST-01 were 0.53 and 0.18 for ST01-T400NH_3 and ST01-T600NH_3, respectively. Moreover, the specific surface areas between the samples treated with air and those treated with 67% NH_3/air mixture at the same temperatures were less than 10%, a margin that was interpreted as within analytical error. Hence, the reduction of specific surface area was mainly ascribed to the temperature, with little variation due to different annealing atmosphere. In contract, the plasma-treated powder (ST01-P300N_2) did not result in significant difference from the original ST-01, even at a heating temperature of 400°C. It was also observed that the treated TiO_2 products in NH_3 or N_2 atmosphere exhibited a pale yellow coloration as a result of absorption in the visible range (Battiston et al., 2000; Marchand et al., 2001). The complete absence of peaks of rutile, which weakly absorbs in the visible region, in the XRD patterns practically rules out the contribution from rutile phase to the powder coloration.

Table 1. Physical properties of the original and N-doped TiO_2.

Sample	Crystalline phase	Mean particle size (nm)	$S_{a,j}/S_{a,ST-01}$	N content (molar ratio, %)	Bonding form
ST-01	Anatase	10	1.0	0	None
ST01-T400NH_3	Anatase	13	0.53	6.3	N(1s)
ST01-T600NH_3	Anatase	35	0.18	2.8	N(1s)
ST01-T400Air	Anatase	N.M.	0.61	2.5	N(1s)
ST01-P300N_2	Anatase	12	0.98	10.1	Ti-N

The chemical composition of the original and modified TiO_2 was determined by ESCA analysis. The broad-scan XPS pattern reveals the characteristics peaks at a binding energy of Ti2p at 459 eV, indicating that the surface of the TiO_2 samples was Ti^{4+} predominant. The O1s core levels were observed at the peak of 533 eV. The Ti/O ratio was approximately obtained by calculating the peak areas of Ti2p and O1s. This result is conformed to the stoichiometry of TiO_2. As shown in Figure 3, for the thermal-treated powders, the N1s core level located at a binding energy around 400 eV, with no significant peaks at 396 eV which is associated with

the substitutive nitrogen in the form of O-Ti-N bonding (Asahi et al., 2001; Irie et al., 2003a,b). The peak area around 400 eV was significantly larger for the ST01-T400NH_3 sample as compared to that for the ST01-T600NH_3. This result is contrary to those reported by Irie et al. (2003a), who observed that the N-atom concentration (at 396 eV) increased with the annealed temperature between 550°C and 600°C. The studies by Sakthival and Kisch (2003) and Justicia et al. (2003), however, also indicated the absence of the substitutive N-atom (396 eV), even though their N-doped TiO_2 clearly manifested absorption shift into the visible region. By comparison, the plasma-treated ST-01 powders (ST01-P300N_2) clearly exhibited peaks around 396 eV, suggesting a different form of nitrogen doping mechanism between the two approaches. In addition, it appeared that the plasma-treated sample incorporated substantially greater amount of nitrogen into the TiO_2 structure as compared to the thermal-treated samples (10.1% vs. <6.3%).

Optical Property

Figure 4 shows the absorption spectra of the original and N-doped ST-01 powders (ST01-T400NH_3 and ST01-P300N_2). Noticeable shift in the absorption band into the visible region was observed for the N-doped samples. However, the degree of photon absorption did not correlate well with the samples calcinated at different temperatures. The experimental results showed that the greatest absorption in both UV and visible regions occurred for ST01-400NH_3, whereas the samples treated with 600° in 67% NH_3/air atmosphere (not shown in the figure) exhibited comparable absorption patterns with the sample treated in air at 400°C. This result, however, was consistent with the tendency of nitrogen contents by XPS analysis, which also indicated that the ST01-T400NH_3 sample contained more nitrogen than other samples (ST01-T600NH_3 and ST01-T400Air, data displayed in Table 1). It was also observed from the figure that the plasma-treated sample exhibited even greater absorptivity over the same spectrum, suggesting a clear “red shift” as a result of effective nitrogen doping. This result appears to be consistent with the superior physical (i.e. specific surface area) and chemical (N doping) properties concerning greater extent of utilization of visible light, possibly suggesting better photocatalytic activity under VIS irradiation.

UV-induced photocatalytic decomposition of IPA

Preliminary experiments involving direct photolysis (without TiO_2) showed that IPA was not oxidized under UV irradiation at 365 nm, and the adsorption of IPA on the glass wall was negligible. Furthermore, since the light source was not activated until the IPA concentration reached a state of equilibrium (i.e. saturation of adsorption capacity of the titania-coated spheres), hence the disappearance of IPA through the reactor was solely due to TiO_2

photocatalysis.

The effect of thermal nitrogen doping on the UV photocatalytic activity of TiO_2 based on the destruction efficiency of IPA is shown in Figure 5. For all cases, approximately 60 minutes of reaction time was needed to reach a steady-state plateau for feed IPA concentration of 1500 ppmv and gas retention time of 20 seconds. The original ST-01 was capable of removing nearly 80% of IPA. In comparison, the removal efficiencies by ST01-T400NH_3 under identical conditions could reach nearly 85%, presenting a slight improvement from the untreated ST-01. However, lower IPA removal efficiencies were noted for both ST01-T600NH_3 (65%) and ST01-T400Air (75%). The efficiency reduction of the former was most likely a result of much lower specific surface area at 600°C calcinations, which directly reduced the surface availability for molecular adsorption and diffusion. On the contrary, the latter sample (ST01-T400Air) possessed similar physical characteristics with ST01-T400NH_3, however its lower absorbance over near-UV range rendered lower photocatalytic activity. This also implies that calcinations by air (80%N_2) were not as effective as by NH_3 (67%) due to the weaker bonding energy of NH_3.

Acetone was detected as the major intermediate product from oxidation of IPA by the original and treated photocatalysts. Initial accumulation of acetone was rapid and reached a plateau after 40 minutes of UV illumination. A secondary intermediate, possibly propylene oxide or mesityl oxide, gradually accumulated as the acetone concentration started to decrease. At the peak of acetone concentration, it was estimated that nearly 50% of the IPA was converted to its intermediate products.

Visible light-induced photocatalytic decomposition of IPA

The IPA destruction efficiencies of ST-01 and ST01-T400NH_3 under visible-light irradiation were shown in Figure 6. Only ST01-T400NH_3 was tested because of its superior material properties and photocatalytic performance under 365-nm irradiation. Also shown as an inset to the figure are the corresponding profiles of acetone concentration.

As noted in the figure, the extents of IPA removals were generally lower than those for UV irradiation – a direct consequence of much weaker absorptivity in the VIS spectrum. Furthermore, the steady-state removal conditions were not attained until approximately 100 minutes of illumination, staging a considerable delay as compared to UV irradiation. More interestingly, the IPA removal efficiencies between the original and calcinated ST-01 were not significantly different, both achieving steady-state efficiencies around 40%. This result is somewhat expected, considering that the photon absorption edges near 400 nm were not substantially different between ST-01 and ST01-T400NH_3 (Figure 4). However, when comparing the extent of intermediate accumulation, it was observed that the acetone

accumulation was significantly less for ST01-T400NH_3, implying the degree of mineralization (i.e. complete conversion to CO_2 as the end product) may be higher. This notion remains to be validated from further experiments.

Batch decomposition study for IPA destruction by the plasma-treated ST-01 under Vis illumination (450nm<λ<550 nm) is currently being conducted. Preliminary results have demonstrated that the ST01-P300N_2 was capable of removing more than 65% of the IPA (feed concentration of 750 ppmv). This result presents an appreciable upgrade from both ST-01 and ST01-T400NH_3. Process optimization is also currently under evaluation for continuous-flow experiments.

REFERENCES

1. Ohno, T.; Mitsui, T.; Matsumura, M. (2003). Photocatalytic activity of S-doped TiO_2 photocatalyst under visible light. *Chem. Lett.*, 32(4), 364-365.
2. Umebayashi, T.; Yamaki, T.; Tanaka, S.; Asai, K. (2003). Visible light-induced degradation of methylene blue on S-doped TiO_2. *Chem. Lett*., 32(4), 330-331.
3. Irie, H.; Watanabe, Y.; Hashimoto, K. (2003). Nitrogen-concentration dependence on photocatalytic activity of $TiO_{2-x}N_x$ powders. *J. Phys. Chem. B*, 107(23), 5483-5486.
4. Irie, H.; Washizuka, S.; Yoshino, N.; Hashimoto, K. (2003). Visible-light induced hydrophilicity on nitrogen-substituted titanium dioxide films. *Chem. Comm.*, 1298-1299.
5. Justicia, I.; Ordejon, P.; Canto, G.; Luis Mozos, J.; Fraxedas, J.; Battison, G.A.; Gerbasi, R.; Figueras, A. (2002). Designed self-doped titanium oxide thin films for efficient visible-light photocatalysis. *Adv. Mater.*, 14(9), 1399-1402.
6. Yu, J.; Yu, J.; Ho, W.; Jiang, Z.; Zhang, L. (2002). Effects of F^- doping on the photocatalytic activity and microstructures of nanocrystalline TiO_2 powders. *Chem. Mater*. 14(8), 3808-3816.
7. Sakthival, S.; and Kisch, H. (2003). Photocatalytic and hotoelectrochemical properties of nitrogen-doped titanium dioxide. *Chemphyschem*, 4, 487-490.
8. Hattori, A.; Yamamoto, M.; Ito, S. (1998). A promoting effect of NH_4F addition on the photocatalytic activity of sol-gel TiO_2 films. *Chem. Lett*. 707-708.
9. Choi, W.Y.; Termin, A.; Hoffmann, M.R. (1994). The role of metal-ion dopants in quantum-size TiO_2 – correlation between photoreactivity and charge-carrier recombination dynamics. *J. Phy. Chem.*, 98(51), 13669-13679.
10. Asahi, R.; Morikawa, T.; Ohwaki, T.; Aoki, K.; and Taga, Y. (2001). "Visible-light photocatalysis in nitrogen-doped titanium oxides," *Science*, 293, 269-271.

11. Battiston, G. A.; Gerbasi, R.; Gregori, A.; Porchia, M.; Cattarin, S.; and Rizzi, G. A. (2000). "PECVD of amorphous TiO_2 thin films: effect of growth temperature and plasma gas composition," *Thin Solid Film*, 371, 126.
12. Marchand, R.; Tessier, F.; Le Sauze, A.; Diot, N. (2001). Typical features of nitrogen in nitride-type compounds. *Int. J. Inorg. Mater.*, 3, 1143-1146.

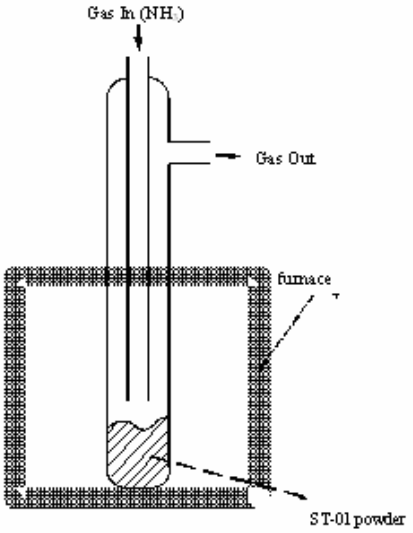

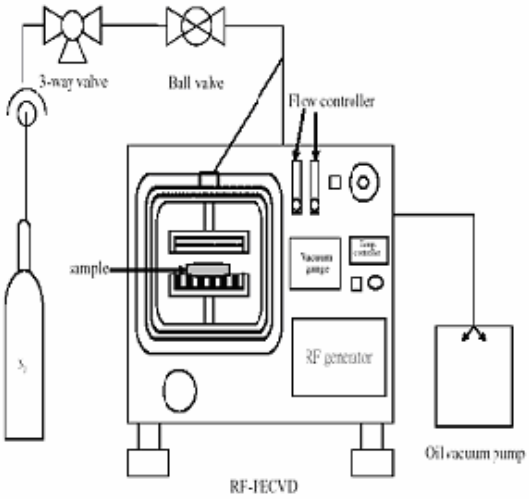

Figure 1. Experimental schematics for nitrogen doping by (a) thermal calcinations, and (b) plasma surface modification.

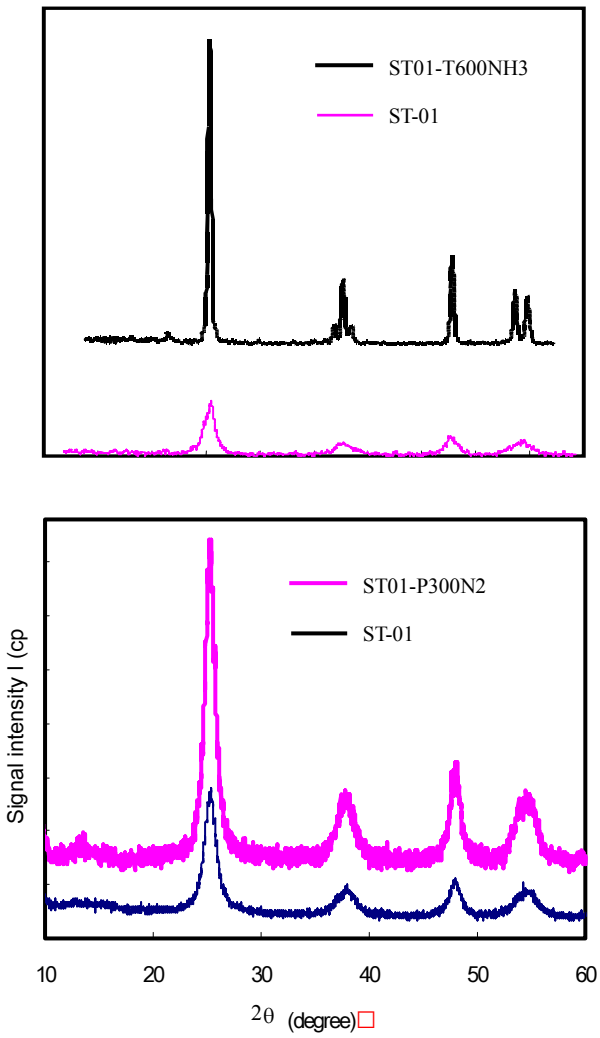

Figure 2. XRD patterns of untreated ST-01 powder vs. (a) thermal ST01-T600NH_3 powder, and (b) plasma ST01-P300N_2 powder.

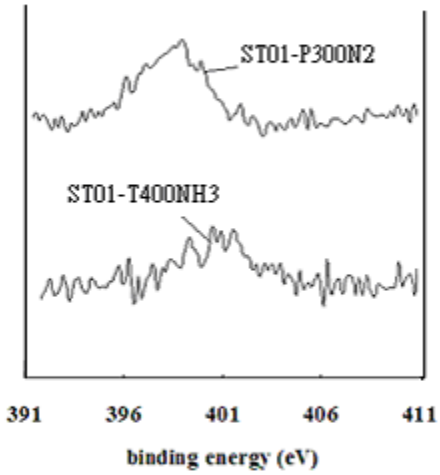

Figure 3. ESCA analyses for the thermal- (ST01-T400NH_3) and plasma-treated (ST01-P300N_2) TiO2 powders.

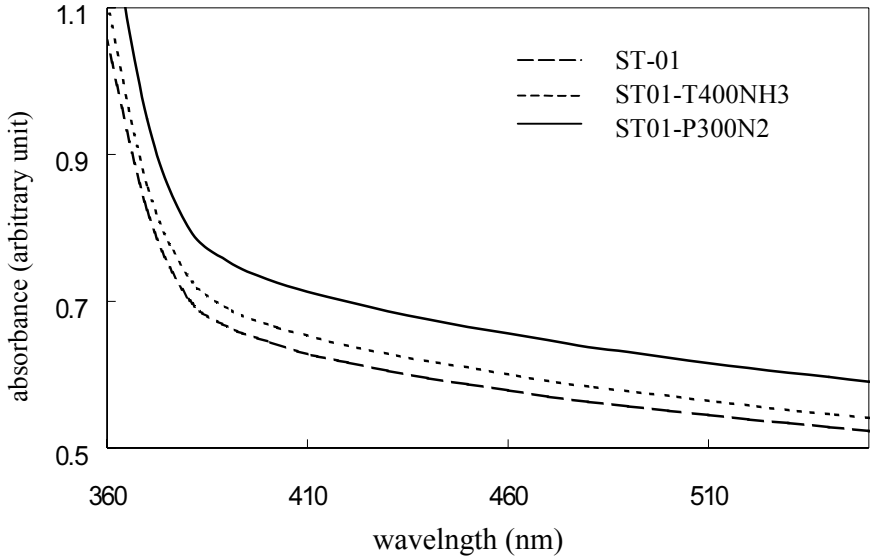

Figure 4. Light absorptivity of the original (ST-01) and treated (ST01-T400NH_3, ST01-P300N_2) TiO_2 powder over near UV and visible ranges.

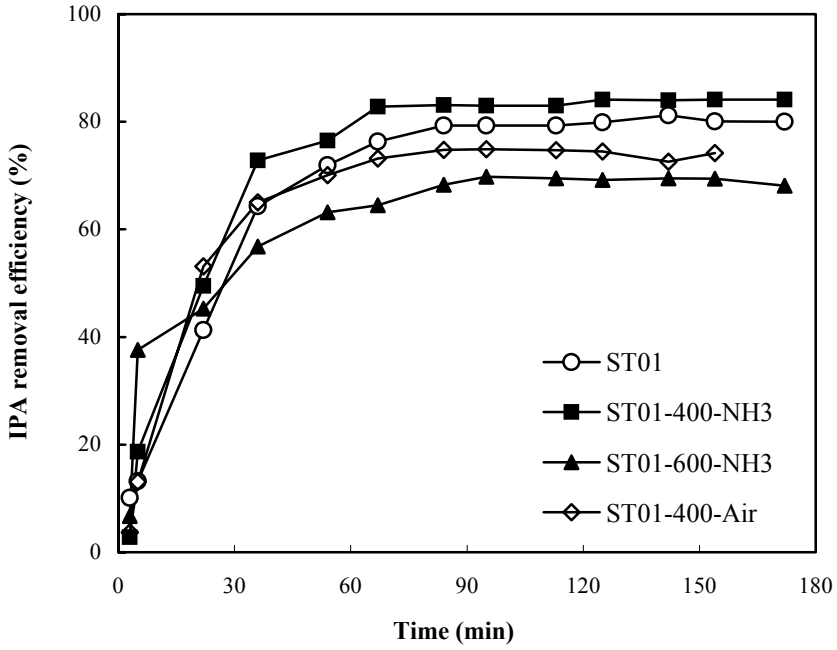

Figure 5. The IPA removal efficiencies by the original and thermal-treated ST-01 powders under UV irradiation at 365 nm.

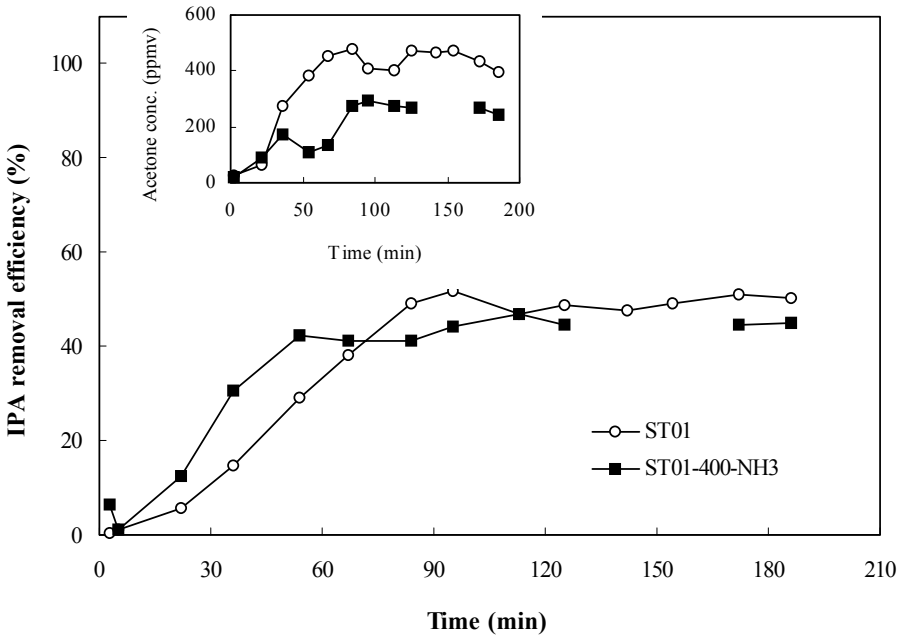

Figure 6. The IPA removal efficiencies by the original and ST01-T400NH_3 powders under fluorescent lamp irradiation. The inset shows the corresponding acetone evolution as a result of IPA oxidation.